3, 20 (1957).
[21]J. T. Vallin and G. D. Watkins, Solid State Commun. 9, 953 (1971).
[22]F. S. Ham, Phys. Rev. 138, A1727 (1965).
[23]The reflection and Raman scattering experiments have been performed in cooperation with J. H. Haanstra (unpublished).
[24]C. H. Henry, S. E. Schnatterly, and C. P. Schlichter, Phys. Rev. 137, A583 (1965).
[25]A good explanation of the satellite lines can not be given but it seems worthwhile to mention an empirical relation we have found to hold between the frequencies of the lines. From the line at the highest energy (2150 cm^{-1}) the other satellites are separated by, respectively, 7, 22, 40, and 75 cm^{-1}. This indicates that possibly a Landé-interval rule holds with $J = 7.5$ cm^{-1} and energies at $E = 0, -J, -3J, -6J, -10J$. Such intervals can be present in spectra of pairs of ions with $S = 2$.
[26]S. Wittekoek and P. F. Bongers, I. B. M. J. Res. Develop. 14, 312 (1970).
[27]T. Coburn, F. Moser, R. Ahrenkiel and K. Teegarden, IEEE Trans. Magnetics MAG-7, 392 (1971).

PHYSICAL REVIEW B VOLUME 7, NUMBER 4 15 FEBRUARY 1973

d-Band Surface States on Transition-Metal Perovskite Crystals: I. Qualitative Features and Application to $SrTiO_3$ †

T. Wolfram, E. A. Kraut, and F. J. Morin
North American Rockwell Science Center, Thousand Oaks, California 91360
(Received 5 July 1972)

The qualitative features of the bulk and surface energy bands of ionic transition-metal perovskite crystals such as $SrTiO_3$, $BaTiO_3$, $KTaO_3$, and $BaZrO_3$ are discussed. The linear-combination-of-atom orbitals (LCAO) method is used in combination with a generalized-Seitz-ionic model to derive parameters for calculating the bulk and surface energy bands. The model for the bulk bands differs in detail from that used by Kahn and Leyendecker for $SrTiO_3$ but is qualitatively similar. Surface energy bands are calculated utilizing the transfer integrals of Kahn and Leyendecker and also those corresponding to the recent results of Mattheiss. In the model, the electrostatic Madelung potentials and ionization potentials have the largest energies. The $(pd\sigma)$ interactions between the d orbitals of transition-metal ions and the p orbitals of the oxygen ions have the next largest energies. The $(pd\pi)$ interactions and the crystalline field splittings follow in magnitude. The $(pp\sigma)$ and $(pp\pi)$ interactions between adjacent oxygen atoms have somewhat higher energy than the spin-orbit interaction. The effective ionic charges are determined by fitting the observed energy gap which is 3–4 eV for these materials. The bulk bands near the energy gap consist of three t_{2g} and two e_g conduction bands and nine valence bands derived from the oxygen p orbitals. The d-conduction-band widths are controlled by the $(pd\pi)$ and $(pd\sigma)$ integrals. The valence-band widths also depend on these parameters but the $(pp\pi)$ and $(pp\sigma)$ integrals add directly to the bandwidth. It is shown that the qualitative features of the energy bands are preserved if the p-p interactions are neglected. In this approximation, analytic results are obtained for the energy bands and the wave functions. Analytic expressions are also derived for the surface-state energy bands for a (001) surface. The perturbations due to spatial variations in the Madelung potentials, change in the electrostatic splitting, variations in the layer spacing, and small rotations in the surface bond angles are included in these analytic expressions. Exact expressions for the spatial variations in the Madelung potentials are derived by a scheme similar to that of Hund for the bulk potentials. The potentials are changed only negligibly except on the surface where changes of the order of several eV occur. The effects of surface irregularities, impurities, and vacancies can easily be treated by the method. Two types of (001) surfaces occur for the ABO_3 perovskite structure. The type-I surface contains oxygen and B ions (the transition-metal ions) while the type-II surface has A and oxygen ions exposed. Formulas for the surface bands of both type surfaces are derived. The dependence of these surface bands on the surface perturbations is discussed. Multiple surface bands and truncated branches which exist only over a certain portion of the Brillouin zone are found to occur. The conduction surface bands follow approximately the dispersion of the bulk band edge. Valence surface bands behave differently for type-I and -II surfaces. The valence surface branch can have a small upward curvature on a type-II surface while for the type-I surface, the dispersion follows the bulk-valence band edge and has a downward curvature as a function of the wave vector parallel to the surface.

I. INTRODUCTION

When a crystalline solid is terminated by a surface, a new set of electronic states appear associated with the surface which are derived from the bulk band structure of the solid. These surface states have considerable technological importance in a variety of areas. Of particular importance

are d-band surface states on transition metals and their compounds which play an important role in such diverse areas as catalysis, electrochemistry, corrosion, hydrogen embrittlement, and lubrication. Unfortunately, however, d-band surface states have eluded detailed study because many of the powerful but simple tools developed for the study of semiconductor surfaces are not applicable to the metals or to the nickel-oxide type of transition-metal compounds.

It appears to us that the requirements for model compounds which will facilitate the study of d-band surface states are met by insulating d-band perovskite compounds such as $SrTiO_3$, $KTaO_3$, or $BaZrO_3$. These materials have empty conduction bands which near the point Γ in the Brillouin zone are nearly pure d band in character. Surface bands derived from these states also have d-band character. As an additional bonus, the occupancy of such surface states can be controlled. They are normally empty but they may be populated by exposing the photoconducting insulator to band-gap or near-bandgap light.

In addition to their surface-state properties, these perovskites have potentially important electro-optic applications in areas such as image storage, photochromism, and electrochromism. Studies of these phenomena in $SrTiO_3$ and other compounds have been reported recently.[1–5]

The purpose of this paper is to establish the qualitative features of surface states on d-band transition-metal perovskite crystals. Our approach is similar to that employed by Levine and Freeman[6] in their treatment of surface states on zinc-blende crystals such as ZnS in the wurtzite phase. It differs in several respects. The number of orbitals necessary to describe the perovskite band structure is large. For ZnS, Levine and Freeman utilized four orbitals; an s orbital for the metal ion and three p orbitals for the anion giving a total of four orbitals. For the perovskite the simplest model requires 14 orbitals; five d orbitals for the B metal ion and nine p orbitals for the three oxygen anions in a unit cell. Despite this complexity we are able to derive simple analytic expressions for both the surface and bulk energy bands including the effects of changes in the Madelung potentials, electrostatic splittings, lattice spacing, and small rotations in bonds at the surface. All or some of these effects probably occur at a real surface. We do not consider perturbations which destroy the two-dimensional periodicity. The inclusion of d orbitals also leads to symmetry effects not present in the zinc-blende crystals. The crystalline field splitting of both d and p levels at the surface differs from that in the bulk. The surface states in the zinc-blende structures are derived from s and p orbitals whereas the class of perovskites studied here have d-like conduction-band surface states. It is this feature which is particularly interesting since the d symmetry of surface states is believed to be an essential factor in accounting for the catalytic activity of transition metals and transition-metal compounds.[7]

It is not the intent of this work to provide a quantitively accurate picture of the energy bands of the d-band perovskites. We are concerned here with providing a qualitative model which treats the largest energies of the system and yields a qualitative description of the nature of the surface energy bands. More sophisticated calculations will undoubtedly be needed as experimental information becomes available. The theory presented here will serve as a basis for further theoretical studies and hopefully will stimulate additional experiments on these interesting materials.

More sophisticated calculations of the energy bands of the perovskites have been discussed recently by Mattheiss[8] and by Soules *et al.*,[9] but the nature of the surface bands has not been previously reported.

The structure of the paper is described now. We begin with a general discussion of the properties of the d-band perovskites in Sec. II. In Sec. III the linear-combination-of-atomic-orbitals (LCAO) model for the bulk bands is described. Analytic expressions for the effective ionic charges are derived in terms of the LCAO parameters and the Madelung potentials. Energy bands are presented for $SrTiO_3$ using a refined version of the Kahn and Leyendecker[10] model. These results are compared with those obtained by utilizing the recent results of Mattheiss.[8] It is then shown that the conduction bands are very nearly unaffected if the small ($pp\pi$) and ($pp\sigma$) interactions between the oxygen atoms are neglected. The qualitative character of the valence bands also remains intact although the approximation is much more serious for these states. Using this approximation, analytic expressions for the bulk energy bands and the wave functions are derived. In Sec. IV the surface-state problem for a (001) surface is formulated. Exact expressions for the spatial variations in the electrostatic potentials are derived. Reductions of the order of 2 eV occur at the surface. One layer inside, the potentials are found to be essentially equal to their bulk values. The changes in the d and p splittings due to the reduction of the crystalline field symmetry at the surface are considered. The three degenerate t_{2g} levels split into a twofold level and a singlet level. Two different types of (001) surfaces occur for the ABO_3 structure. In one case, the surface contains B and oxygen ions, while for the second case A and oxygen ions are on the surface. Analytic formulas are derived for the energies and wave functions of the surface states for both types

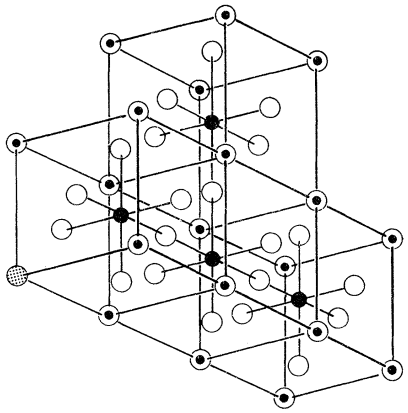

FIG. 1. ABO_3 cubic perovskite structure. Dark circles represent the B ions, open circles represent the oxygen ions, and the dotted circles indicate the A ions.

of surfaces including the effects of changes in Madelung potentials, splittings, lattice spacing, and small rotations of the B-metal–oxygen bonds at the surface. A series of surface bands for both types of (001) surface are presented which show how these states depend upon the surface perturbations.

Finally, in Sec. V we summarize our results and present some conclusions and a discussion of future work.

II. GENERAL FEATURES OF d-BAND PEROVSKITES

The cubic perovskites (space group O_h^1, $Pm3m$) crystals are of the ABO_3 type where A and B are metal cations and O is an oxygen ion. The perovskite structure is shown in Fig. 1. The A and B ions are surrounded by octahedra of oxygen which produce a cubic ligand field. The oxygen ions, however, experience an axial field produced by the noncubic distribution of the A- and B-metal ions. We shall be mainly interested in a subclass of the perovskites which have transition-metal ions with d orbitals in the B sites and larger metal ions with s orbitals in the A sites. The compounds $SrTiO_3$, $KTaO_3$, $BaZrO_3$, and $BaTiO_3$ (in the high-temperature cubic phase above the ferroelectric transition) are typical examples. The ligand field causes a splitting of the fivefold degenerate d states into the familiar threefold t_{2g} and twofold e_g levels. The three degenerate oxygen p states are split by the axial crystal field into a twofold level and a singlet.

The bonding in these crystals is highly ionic. The lowest empty electron orbitals and the ideal ionic charges of the A and B ions are indicated in Table I. The ionization potentials for the free ions[11] and the electron affinity[12] of oxygen are also given in Table I. The crystals are not completely ionic and the covalency effects are important in determining electronic properties such as crystal field effects and the energy gap. A small amount of covalency leads to large changes in the electrostatic Madelung potentials. Energy gaps on the order of 15 eV would be predicted if these perovskites were fully ionic whereas gaps of 3–4 eV are observed or expected. Kahn and Leyendecker[11] have calculated the energy bands of $SrTiO_3$ using a simple LCAO model together with Seitz's ionic model.[13] They find that the ionic gap of 15 eV is reduced to about 3 eV when the effective ionic charges are reduced by 15%. Augmented-plane-wave (APW) calculations by Mattheiss[8] yield a band gap of about 6.2 eV. These APW results were utilized to obtain a set of LCAO parameters. When these parameters are adjusted to fit optical data, a gap of 3.5 eV results. A large band gap (~11 eV) has been found by Soules *et al.*[9] These authors argue that the small observed band gap results from strong correlation or exciton effects which invalidate the energy band calculation of the excited-state energies. Numerous transport experiments, however, argue strongly that these effects are not of prime importance.

The features of the band structure of strontium titanate are representative of the class of perovskites considered here. The largest energies are those resulting from the Madelung and ionization potentials. The Madelung energies are substantially reduced by covalency effects. The energy bands within a few volts of the energy gap are characterized by five (empty) conduction bands derived from the d orbitals of the B-transition-metal ion while the nine (filled) valence bands originate from the three $2p$ orbitals on each of the three oxygen ions. The s states associated with the B-metal ions are expected to lie at much higher energies and do not contribute strongly to the band structure near the gap. The energy gap is 3–4 eV. The next most important energy is the p-d interaction which produces conduction- and valence-band widths of 3–4 eV. The wave functions for states away from Γ in the Brillouin zone are admixtures of p and d orbitals. The mixing decreases with increasing energy gap. Finally, the p-p interactions between adjacent oxygens lead to a modification of the valence band near the gap but have little effect on the d conduction bands. Nonorthogonality effects, the effects of more distant orbital interactions, spin-orbit interactions, polaron and exciton effects, and the use of additional orbitals are important in an accurate LCAO calculation of the energy bands. The qualitative features, however, are not expected to depend strongly on such effects.

Strontium Titanate

Strontium titanate possesses an amazing variety of interesting properties. In its pure state, it is an insulator transparent to visible light. At high

TABLE I. Lowest empty-electron orbitals and energy necessary to ionize electrons from the levels for the free ions. Columns 3 and 5 give the charge of the free ion. Oxygen O^{2-} has $2p^3$ and the electron affinity of O^- is 9.22 eV (see Ref. 5). Ionization potentials are taken from Ref. 4.

Crystal ABO_3	A orbital	A charge	A ionization potential (eV)	B orbital	B charge	B ionization potential (eV)
$SrTiO_3$	$5s$	2^+	−11.03 (II)	$3d$	4^+	−43.24 (IV)
$BaTiO_3$	$6s$	2^+	−10.00 (II)	$3d$	4^+	−43.24 (IV)
$KTaO_3$	$4s$	1^+	−4.34 (I)	$5d$	5^+	−57.0[a] (V)
$BaZrO_3$	$6s$	2^+	−10.00 (II)	$4d$	4^+	−34.33 (IV)

[a]Estimated from the Mo series.

temperatures, it is cubic but undergoes a transition to a tetragonal structure[14–18] at about (105–110) °K. The temperature dependence of the dielectric constant suggests that a ferroelectric transition should occur at 45 °K. However, no discontinuity in the dielectric constant is observed.[19,20]

When strontium titanate is reduced it takes on a blue color. It displays a number of interesting photochromic and electrochromic properties[1–4] when doped with metal ions. Doped strontium titanate is also a superconductor[21] with a transition temperature of about 0.3 °K.

The transport properties are complex due to defect contributions[22,23] and the effects of phase transitions. The electrical conductivity, Hall, and Seebeck coefficients were first measured by Frederikse *et al.*[24] in reduced $SrTiO_3$. More recent measurements of the Hall effect and photoconductivity of pure and doped $SrTiO_3$ have been reported.[25,26] Anomalies in the photoconductivity and Hall effect have been interpreted by Yasunaga and Nakado[25] as evidence for a small amount of ferroelectric phase in an otherwise paraelectric host.

Optical-absorption measurements on transition-metal ions in $SrTiO_3$ have been reported by Gandy[27] and more recently by Müller.[28] Raman spectra have been reported by Narayanan and Verdam.[29] Numerous electron-paramagnetic-resonance studies have been reported[30,31] and thermally stimulated current measurements have been performed.[32] In the cubic phase, the lattice spacing[33] is 3.90 Å. The energy gap has been studied by Blazey[34] using wavelength-modulation spectroscopy. Direct transitions from the valence band to the conduction band at the point Γ in the Brillouin zone give a gap of 3.34 eV. The indirect band gap between the maximum at Γ in the valence band to the minimum in the conduction band at the point X at the corner of the Brillouin zone was reported to be 3.24 eV for the cubic phase (see Fig. 2). In the tetragonal phase, Blazey found an indirect band gap of 3.28 eV. The reflectance spectra of both $SrTiO_3$ and $BaTiO_3$ have been reported by Cardona[35] and that of $KTaO_3$ by Kurtz.[36] Calculations by Kahn and Leyendecker predict equienergy contours in the form of six ellipsoidal surfaces at the point X (Fig. 2) when spin-orbit effects are included. It is not completely certain that the minimum gap occurs at the point X, although magnetoresistance measurements[37] support the (100) ellipsoidal model. Piezoresistance measurements, however, favor a direct band gap.[38] APW calculations by Mattheiss[8] also indicate a direct gap. Magnetoresistance measurements on $KTaO_3$ have also been reported which support the ellipsoidal model.[39] The effective mass of electrons in n-type $SrTiO_3$ has been measured by a variety of techniques including the Hall effect,[24,40] magnetic susceptibility,[41] tunneling,[42] Shubnikov–de Haas,[43] and heat capacity measurements.[44,45] Different measurements give different types of effective masses but $m^* \sim 5m$ to $6m$ appears to be representative for $SrTiO_3$. Results for $KTaO_3$ indicate that $m^* \lesssim m$ in n-type material.[40,42,46–48]

III. BULK ENERGY BANDS

In this section we discuss a simple LCAO model for the energy bands of the d-band perovskite structures. The important parameters are dis-

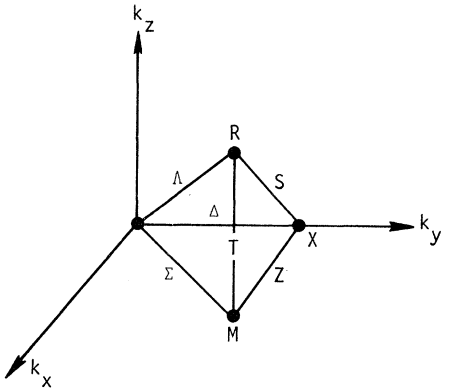

FIG. 2. First Brillouin zone for the simple cubic structure. The symmetry points and lines are defined by $\Gamma = (0,0,0)$. $x = \pi/2a(0,1,0)$, $M = \pi/2a(1,1,0)$, $R = \pi/2(1,1,1)$, $\Delta = \pi/2a(x,1,0)$, $\sum = \pi/2a(\chi,\chi,0)$, $T = \pi/2a(1,1,x)$, $\Delta = \pi/2a(x,x,x)$, $S = \pi/2a(x,1,x)$, where a is the oxygen–B-metal ion separation.

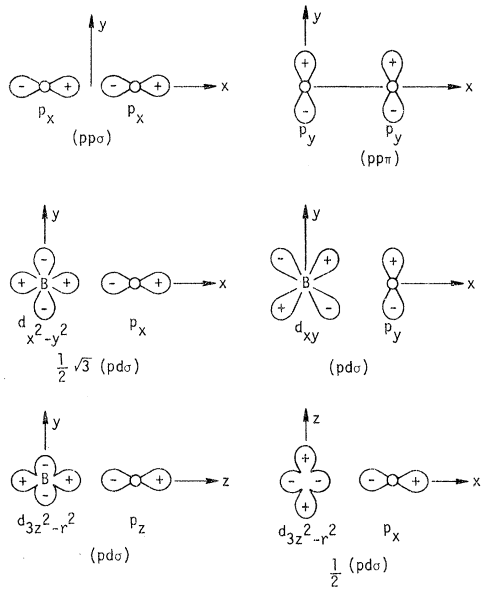

FIG. 3. Schematic representation of the off-diagonal σ and π transfer integrals.

cussed and simple approximate analytic formulas are derived which describe the qualitative features of the band structure. The approach discussed here follows closely that used by Kahn and Leyendecker[10] in their treatment of $SrTiO_3$. The energy bands differ from those obtained by Kahn and Leyendecker because of different effective charges, a refined treatment of the energy-gap determination, the use of more accurate values of the electron affinity, and different values of $(pp\pi)$ and $(pp\sigma)$.

The application of the LCAO method to the energy bands of solids introduced by Slater and Koster[49] has been widely used in recent years as an interpolation scheme for deriving energy bands based upon more accurate calculations at high symmetry points.[8,50]

In the LCAO method, the Bloch states are linear combinations of the atomic orbitals relevant to the solid under consideration. In the case of the d-band perovskites, these are the orbitals listed in Table I. The method is physically appealing because the important parameters are easily visualized in terms of atomic orbitals and their transfer integrals. In addition, the resulting description fits naturally into chemical descriptions of surface reactions.

The LCAO method has been discussed in detail in several articles[8,10,50-52] so we present here only the results. The Bloch wave functions $\psi(\vec{k})$ are constructed from linear combinations of the five d orbitals of the B-transition-metal ion and the three p orbitals of each of the three oxygen atoms in each unit cell giving a total of 14 orbitals. The s orbitals of the A-metal ions are assumed to be unimportant for the energy bands near the gap since they have higher energies. The model Hamiltonian consists of the kinetic energy plus a sum of effective local potentials. The effects of the long-range electrostatic potential are accounted for approximately by including in the diagonal matrix elements a series expansion of the total field about each lattice site.[10]

The transfer integrals considered in our model of the d-band perovskites include the diagonal interactions between d orbitals (p orbitals) on the same atom, the $(pd\sigma)$ and $(pd\pi)$ transfer integrals between neighboring oxygen and B-metal atoms, and the $(pp\sigma)$ and $(pp\pi)$ interactions between adjacent oxygen atoms. The orbitals involved in the nondiagonal interactions are illustrated schematically in Fig. 3. The orbitals are denoted by the symmetry of the angular component of the wave function.

The diagonal matrix elements for the d orbitals are

$$\begin{aligned} &E_t = \epsilon_d + V_M^{(B)} + V_t \quad \text{for } d_{xy},\ d_{xz}, \text{ and } d_{yz}, \\ &E_d + \epsilon_d + V_M^{(B)} + V_e \quad \text{for } d_{3z^2-r^2} \text{ and } d_{x^2-y^2}, \end{aligned} \tag{1}$$

where ϵ_d is the ionization energy of an electron on the free-B-metal ion, $V_M^{(B)}$ is the Madelung potential at the B-metal–ion site, and v_t and v_e are the electrostatic shifts in the energies of the t_{2g} (d_{xy}, d_{yz}, and d_{xz}) and e_g ($d_{3z^2-r^2}$ and $d_{x^2-y^2}$) levels due to the cubic crystalline field. The t_{2g} levels are lowered in energy by v_t, the e_g levels are raised in energy by v_e, and group-theoretical arguments show that $v_e/v_t = -\frac{6}{4}$. The quantity $v_e - v_t$ is the total splitting of the d levels at the point Γ in the Brillouin zone. This splitting is smaller than the $10Dq$ obtained from a molecular-orbital calculation.[53] Mattheiss[8,50] has discussed the relation of the molecular-orbital crystal field splitting to the splitting entering into a LCAO band calculation. In strontium titanate[10] $10Dq$ is believed to be about 2.4 eV. According to Kahn and Leyendecker[10] $v_e - v_t$ is 0.62 eV, while the splitting at Γ deduced by Mattheiss is very nearly equal to $10Dq$. For the p orbital the diagonal energies are

$$\begin{aligned} &E_{\parallel} = \epsilon_p + V_M^{(O)} + v_{\parallel} \quad \text{for } p_{\parallel}, \\ &E_{\perp} = \epsilon_p + V_M^{(O)} + v_{\perp} \quad \text{for } p_{\perp}, \end{aligned} \tag{2}$$

where ϵ_p is the electron affinity of O^-, $V_M^{(O)}$ is the Madelung potential at an oxygen site, and $v_{\parallel}$ and $v_{\perp}$ are the electrostatic shifts due to the axial crystalline field. p orbitals directed towards the nearest-neighbor B ion are denoted by $p_{\parallel}$ while those directed perpendicular are denoted by $p_{\perp}$. The $p_{\parallel}$ levels are lowered by $v_{\parallel}$ relative to $\epsilon_p + V_M^{(O)}$ and the $p_{\perp}$ levels are raised by $v_{\perp}$. The total splitting at Γ is estimated to be 0.48 eV for $SrTiO_3$ by Kahn

and Leyendecker while application of this model to the results of Mattheiss gives a much smaller value.

At the point Γ the conduction-band energies are E_e (twofold), E_t (threefold), and the valence-band energies (all of which are threefold degenerate) are

$$E_{p1}^{\Gamma} = E_{\perp} - 4(pp\pi),$$
$$E_{p2,p3}^{\Gamma} = \tfrac{1}{2}[E_{\perp} + E_{\parallel} + 4(pp\pi)] \pm r, \tag{3}$$
$$r = \{[\tfrac{1}{2}(v_{\parallel} - v_{\perp}) - 2(pp\pi)]^2 + 8[(pp\sigma) + (pp\pi)]^2\}^{1/2}.$$

The direct band gap Δ is given by

$$\Delta = E_t - E_{p2}^{\Gamma} \equiv \Delta_0 + \delta,$$
$$\Delta_0 = \epsilon_d - \epsilon_p + V_M^{(B)} - V_M^{(O)}, \tag{4}$$
$$\delta = -[2(pp\pi) - v_t + \tfrac{1}{2}(v_{\parallel} + v_{\perp}) + r].$$

In Eq. (4), the gap Δ is decomposed into a term which depends on the ionization potential, electron affinity, and electrostatic Madelung potentials but not on the $(pp\pi)$ or $(pp\sigma)$. The second term δ accounts for the p-p interactions and the electrostatic splitting but does not depend upon the Madelung potentials. This decomposition will prove useful in determining the effective charges of the ions.

A. Madelung Potentials for Perovskites

The Madelung potentials at the various lattice sites for arbitrary effective ionic charges can easily be obtained using the method of Hund.[54] Utilizing this method we find that for the perovskite structure

$$V_M^{(A)} = -(e^2/2a)[q(B)\psi(\tfrac{1}{2}, \tfrac{1}{2}, \tfrac{1}{2}) - 3q(O)\psi(\tfrac{1}{2}, \tfrac{1}{2}, 0) + q(A)\psi(0, 0, 0)],$$
$$V_M^{(B)} = -(e^2/2a)[q(B)\bar{\psi}(0, 0, 0) - 3q(O)\psi(\tfrac{1}{2}, 0, 0) + q(A)\psi(\tfrac{1}{2}, \tfrac{1}{2}, \tfrac{1}{2})], \tag{5}$$
$$V_M^{(O)} = -(e^2/2a)\{q(B)\psi(\tfrac{1}{2}, 0, 0) - q(O)[\bar{\psi}(0, 0, 0) + 2\psi(\tfrac{1}{2}, \tfrac{1}{2}, 0)] + q(A)\psi(\tfrac{1}{2}, \tfrac{1}{2}, 0)\},$$

where a is the Ti-oxygen separation and $q(A)$, $q(B)$, and $q(O)$ are *magnitudes* of the effective ionic charges on the A, B, and O ions. The quantities $\psi(r, s, t)[\bar{\psi}(0, 0, 0)]$ are Hund potentials [self-potential] for the neutralized cubic lattice:

$$\psi(\tfrac{1}{2}, 0, 0) = -0.095932,$$
$$\psi(\tfrac{1}{2}, \tfrac{1}{2}, 0) = -0.582522,$$
$$\psi(\tfrac{1}{2}, \tfrac{1}{2}, \tfrac{1}{2}) = -0.801936, \tag{6}$$
$$\bar{\psi}(0, 0, 0) = -2.837298.$$

Charge neutrality requires that $q(A) + q(B) - 3q(O) = 0$. From Eq. (4) it is clear that the energy gap Δ_0 depends directly upon the effective charges on the ions. For $SrTiO_3$, Kahn and Leyendecker found that a reasonable energy gap resulted if the charge on oxygen was decreased from $-2|e|$ to about $-1.7|e|$. The effective charge on the Ti ion was reduced to about $+3.1|e|$ and the Sr charge was left at $+2|e|$. Variations in the Sr charge were relatively less important. For reasons associated with charge neutrality of free surfaces (to be discussed later), we shall assume that the ratios of the charges remain the same as in the fully ionic case. This leads to only slight changes in the ionicity from that determined by Kahn and Leyendecker.

The effective charges can be expressed in terms of the Hund potentials, electrostatic splitting, ionization potential, electron affinity, observed energy gap, and the quantities $(pp\pi)$ and $(pp\sigma)$. For example, for the ABO_3 perovskites such as $SrTiO_3$, $BaTiO_3$, and $BaZrO_3$, where $q(A) = q(O) = \frac{1}{2}q(B)$, one finds, using Eq. (5), that

$$q(O) = \frac{\Delta - (\epsilon_d - \epsilon_p) + [2(pp\pi) - v_t + \frac{1}{2}(v_{\parallel} + v_{\perp}) + r]}{4.708345\, e^2/2a}. \tag{7}$$

B. Qualitative Features of Bulk Energy Bands

The qualitative features of the bulk bands can be obtained easily in the approximation that $(pp\sigma) = (pp\pi) = 0$. For this approximation, the secular-matrix-equation block diagonalizes into three 3×3's which we denote by M_{xy}, M_{xz}, and M_{yz} and a 5×5 M_{xyz}. The blocks $M_{\alpha\beta}$ are of the form

$$M_{\alpha\beta} = \begin{pmatrix} E_t - E & 2i(pd\pi)S_{\alpha} & 2i(pd\pi)S_{\beta} \\ -2i(pd\pi)S_{\alpha} & E_{\perp} - E & 0 \\ -2i(pd\pi)S_{\beta} & 0 & E_{\perp} - E \end{pmatrix} \times \begin{pmatrix} c_{\alpha\beta} \\ c_{\alpha} \\ c_{\beta} \end{pmatrix} = 0, \tag{8}$$

where the coefficients $c_{\alpha\beta}$, c_{α}, and c_{β} are the amplitudes of the orbitals $d_{\alpha\beta}$, p_{α}, and p_{β} which make up the approximate eigenstates. For example, when $\alpha\beta = xy$, then $c_{\alpha\beta}$ is the amplitude of the d_{xy} d orbital on the B-metal ion, c_{α} and c_{β} are the amplitudes of the p orbitals $p_x^{(2)}$ and $p_y^{(1)}$. In Eq. (8), $S_{\alpha} = \sin k_{\alpha}a$, $c_{\alpha} = \cos k_{\alpha}a$, where $\alpha = x$, y, and z, a is the B-ion–oxygen distance, and k_{α} are the components of the wave vector. The superscripts (1), (2), and (3) on the p orbitals are used to indicate the oxygen sites displaced from the B-metal site by $a(1, 0, 0)$, $a(0, 1, 0)$, and $a(0, 0, 1)$, respectively. For $\alpha\beta = xz$, the amplitudes are for d_{xz}, $p_x^{(3)}$, and $p_z^{(1)}$ and for $\alpha\beta = yz$, the amplitudes are for d_{yz}, $p_y^{(3)}$, and $p_z^{(2)}$. The oxygen orbitals

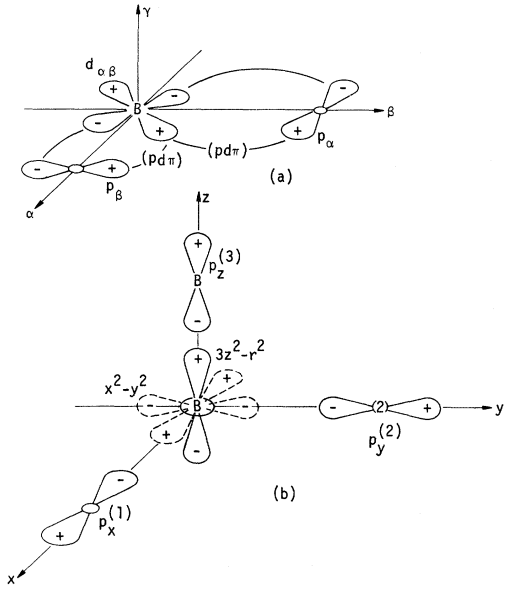

FIG. 4. Orbitals involved in the wave functions: (a) for the 3×3 blocks, (b) for the 5×5 block.

involved are those which have a $(pd\pi)$ interaction with the d orbital $d_{\alpha\beta}$ as shown schematically in Fig. 4(a). It is evident that only the t_{2g} orbitals and the $p_\perp$ orbitals are involved in these wave functions. The eigenvalues are

$$E_1^{\alpha\beta} = E_\perp ,$$
$$E_{(2,3)}^{\alpha\beta} = \tfrac{1}{2}(E_t + E_\perp) \pm \{[\tfrac{1}{2}(E_t - E_\perp)]^2 + 4(pd\pi)^2(S_\alpha^2 + S_\beta^2)\}^{1/2} . \quad (9)$$

The (unnormalized) eigenvectors $\psi_i^{\alpha\beta}$ corresponding to these eigenvalues are

$$\psi_1^{\alpha\beta} = \begin{pmatrix} 0 \\ S_\beta \\ -S_\alpha \end{pmatrix} ,$$
$$\psi_{(2,3)}^{\alpha\beta} = \begin{pmatrix} E_\perp - E_{(2,3)}^{\alpha\beta} \\ 2i(pd\pi)S_\alpha \\ 2i(pd\pi)S_\beta \end{pmatrix} . \quad (10)$$

From Eq. (9) it can be seen that there are three valence bands with constant energy $E_\perp$ whose wave functions are particular admixtures of oxygen p orbitals. In the approximation that $(pp\sigma)$ and $(pp\pi)$ vanish, these states do not mix with the d orbitals.

There are also three equivalent pairs of branches with two-dimensional dispersion (i.e., dependent only on two components of the k vector). The $E_2^{\alpha\beta}$ branch is a conduction band and the $E_3^{\alpha\beta}$ branch is a valence band. At Γ, one of the pair is a pure p state and one is a pure d state. Near Γ, the dispersion is quadratic:

$$E_{(2,3)}^{\alpha\beta} \approx \left(\frac{E_t}{E_\perp}\right) \pm \frac{4(pd\pi)^2(K_\alpha^2 + K_\beta^2)a^2}{E_\perp - E_t} ,$$
$$\psi_3^{\alpha\beta} \approx \begin{pmatrix} 2(pd\pi)(S_\alpha^2 + S_\beta^2)(E_\perp - E_t)^{-1} \\ iS_\alpha \\ iS_\beta \end{pmatrix} , \quad (11)$$
$$\psi_2^{\alpha\beta} \approx \begin{pmatrix} E_\perp - E_t \\ 2i(pd\pi)S_\alpha \\ 2i(pd\pi)S_\beta \end{pmatrix} .$$

The ratio of the d-orbital amplitude to the p-orbital amplitude in $\psi_3^{\alpha\beta}$ is linear in the two-dimensional wave vector, and the admixture of p orbitals into $\psi_2^{\alpha\beta}$ is also linear in the two-dimensional wave vector.

The 5×5 block involves the e_g d orbitals and the $p_\parallel$ (p orbitals directed into the nearest-neighbor B ion) orbitals. The orbitals involved in these states are shown schematically in Fig. 4(b). The d orbitals are the e_g type and the p orbitals are the $p_\parallel$ type. They are coupled by the $(pd\sigma)$ interaction. The eigenvalues are

$$E_1^{xyz} = E_\parallel ,$$
$$E_{2,3,4,5}^{xyz} = \tfrac{1}{2}(E_e + E_\parallel) \pm \{[\tfrac{1}{2}(E_e - E_\parallel)]^2 + 2(pd\sigma)^2[(S_x^2 + S_y^2 + S_z^2) \pm S^2]\}^{1/2} , \quad (12)$$

where

$$S^2 = (S_x^4 + S_y^4 + S_z^4 - S_x^2S_y^2 - S_x^2S_z^2 - S_y^2S_z^2)^{1/2} .$$

In Eq. (12) the choice of signs is $(++)$ for E_2^{xyz}, $(+-)$ for E_3^{xyz}, $(-+)$ for E_4^{xyz}, and $(--)$ for E_5^{xyz}. The corresponding eigenvectors are

$$\psi_1^{xyz} = \begin{pmatrix} 0 \\ S_xS_y \\ 0 \\ S_yS_z \\ S_xS_z \end{pmatrix} , \quad (13)$$

$$\psi_\alpha^{xyz} = \begin{pmatrix} (E_\parallel - E_\alpha^{xyz})(S_y^2 - S_z^2) \\ 2i(pd\sigma)S_z(S_y^2 - S_x^2) \\ \dfrac{[x_\alpha(pd\sigma) - 4(pd\sigma)^2(S_z^2 - S_x^2 - S_y^2)](E_\parallel - E_\alpha^{xyz})}{\sqrt{3}\,(pd\sigma)^2} \\ iS_x[x_\alpha - (pd\sigma)^2(4S_z^2 - 2S_y^2)] \\ -iS_y[x_\alpha - (pd\sigma)^2(4S_z^2 - 2S_x^2)] \end{pmatrix} , \quad (14)$$

where $x_\alpha = (E_\parallel - E_\alpha^{xyz})(E_e - E_\alpha^{xyz})/(pd\sigma)$ and $\alpha = 2, 3, 4,$

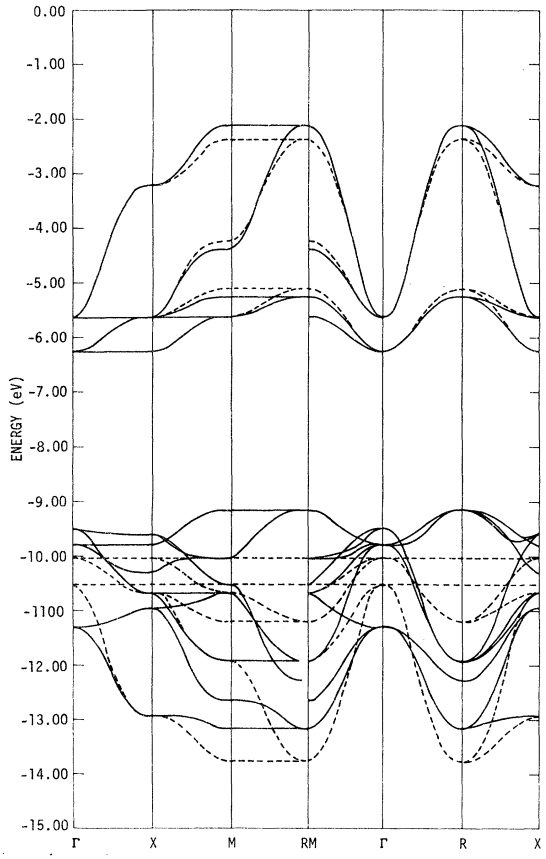

FIG. 5. Energy bands for $SrTiO_3$. The solid curves are calculated using the parameters (in eV) $E_t = -6.258$, $E_e = -5.638$, $E_\perp = -10.039$, $E_\parallel = -10.519$, $(pd\sigma) = 2.1$, $(pd\pi) = 0.84$, $(pp\sigma) = 0.379$, and $(pp\pi) = -0.062$. The dashed curves are for the same parameters except $(pp\sigma) = (pp\pi) = 0$.

and 5. It can easily be seen by considering the point Γ that $E^{xyz}_{2,3}$ are conduction bands formed from B-metal ion e_g d orbitals. $E^{xyz}_{1,4,5}$ are valence bands formed from oxygen orbitals.

C. Bulk Energy Bands of $SrTiO_3$

The results of the preceding sections can be used to obtain the energy bands of strontium titanate. We shall first discuss a modification of the energy-band model of Kahn and Leyendecker. A second model is developed by choosing transfer integrals to fit the results of Mattheiss. Surface energy bands are then calculated using these results.

Kahn and Leyendecker utilized the values (in electron volts) $(pd\sigma) = 2.1$, $(pd\pi) = 0.84$, $v_t = -0.248$, $v_e = 0.372$, $v_\parallel = -0.32$, and $v_\perp = 0.16$. We use Switendick's[55] values $(pp\sigma) = 0.379$ and $(pp\pi) = -0.062$. In addition, we use Blazey's value of 3.24 eV for the energy gap. Then Eq. (7) gives $q(O) = 1.6314 = q(Sr)$, $q(Ti) = 3.2628$. The Madelung potentials calculated from Eq. (5) are $V_M^{(Sr)} = 16.2042$, $V_M^{(O)} = -19.4187$, and $V_M^{(Ti)} = 37.2303$. Combining these with the ionization potentials and electron affinity given in Table I, we find that $E_t = -6.258$, $E_e = -5.638$, $E_\perp = -10.039$, and $E_\parallel = -10.519$. The strontium level has an energy $E_{Sr} = 5.174$. It is therefore about 11.5 eV above the Ti level. For this reason we are justified in neglecting the effects of the strontium 5s level on the energy bands near the gap. These values differ from those used by Kahn and Leyendecker. The differences result from a variety of reasons: (i) their value of $q(O)$ was about 1.68 and $q(Sr)$ was 2, (ii) their Madelung potentials were slightly in error, (iii) they did not include the effects of electrostatic splitting or $(pp\pi)$ and $(pp\sigma)$ in determining $q(O)$ from the energy gap, (iv) different values for the electron affinity were used, and (v) the correct[56] values of Switendick's $(pp\sigma)$ and $(pp\pi)$ parameters were used.

The energy bands calculated for $SrTiO_3$ using the LCAO parameters derived above are indicated by the solid curves in Fig. 5. They are qualitatively similar to those calculated by Kahn and Leyendecker. The lower conduction band is composed of t_{2g} d orbitals near Γ. Away from Γ, the $p_\perp$ orbitals mix with the t_{2g} orbitals because of the $(pp\pi)$ interactions. Near the end of the Brillouin zone (R), the wave functions are about 85% t_{2g} and 15% $p_\perp$. The bandwidth is controlled by $(pd\pi)$ as indicated by Eq. (9). The splitting of the t_{2g} and e_g conduction bands is $v_e - v_t = 0.62$ eV. The e_g bandwidth is controlled by $(pd\sigma)$ as indicated by Eq. (12). The mixture of orbitals at R is about 70% e_g and 30% $p_\parallel$. The valence bands are split at Γ by both the axial crystal field and the $(pp\pi)$ and $(pp\sigma)$ interactions [see Eq. (13)]. The bandwidth of the upper valence band is controlled by $(pd\pi)$, $(pp\sigma)$, and $(pp\pi)$. The lower valence-band width is determined by $(pd\sigma)$.

If $(pp\sigma)$ and $(pp\pi)$ are assumed to vanish, then we obtain the energy bands indicated by the dashed curves of Fig. 5. The only significant changes are in the valence bands. The narrow bands are now flat. It is clear that the conduction bands are essentially unaffected by $(pp\sigma)$ and $(pp\pi)$. The valence bands are modified more significantly since the p-p interactions prevent the formation of flat bands.

The t_{2g} and e_g bands are coupled only indirectly through the p-p interactions. Since these interactions are weak, the coupling between the bands is weak. This suggests that virtual d-band surface states may occur near the e_g band edge which lies in the t_{2g} continuum of states.

A more sophisticated LCAO model for $SrTiO_3$ has been derived by Mattheiss[8] based on APW calculations and optical data for $SrTiO_3$. We have determined the parameters of our model by fitting

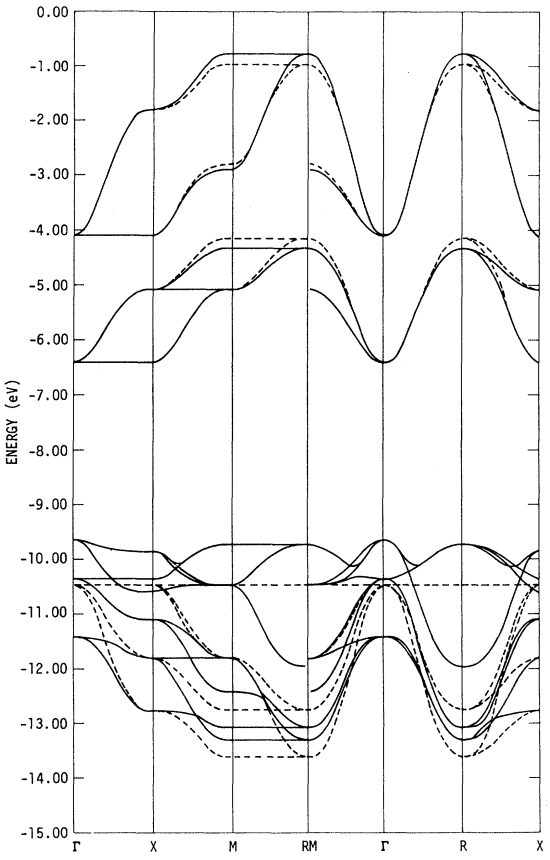

FIG. 6. Energy bands for $SrTiO_3$. The solid curves are calculated using the parameters (in eV) $E_t = -6.407$, $E_e = -4.097$, $E_\perp = -10.473$, $E_\parallel = -10.473$, $(pd\sigma) = -2.23$, $(pd\pi) = 1.337$, $(pp\sigma) = 0.341$, and $(pp\pi) = -0.03$. The dashed curves are for the same parameter except $(pp\sigma) = (pp\pi) = 0$.

to a number of key points. We require our model to match the p and d bandwidths at X and match the p and d levels at Γ. We use, however, an energy gap of 3.24 eV. The electrostatic considerations of our model fix the absolute energy of the energy bands, a feature not present in Mattheiss's LCAO model. The parameters obtained are $q(O) = 1.654$, and (in electron volts) $E_t = -6.407$, $E_e = -4.097$, $E_\perp = -10.473$, $E_\parallel = -10.473$, $(pd\pi) = 1.337$, $(pd\sigma) = -2.23$, $(pp\pi) = -0.03$, and $(pp\sigma) = 0.341$. The energy bands for these parameters are indicated in Fig. 6 by the solid curves. These bands agree qualitatively with those of Mattheiss over the entire Brillouin zone. This indicates that the overlap effects can be adequately treated by modifying the transfer integrals. The agreement with the parameters used by Mattheiss indicates that these modifications are small. For example, Mattheiss uses $(pd\sigma) = -2.25$, $(pd\pi) = 1.14$, $(pp\sigma) = 0.425$, and $(pp\pi) = -0.107$. It is noted that the values deduced for $(pp\pi)$ and $(pp\sigma)$ are similar to those of Switendick. The effective charges for both of our calculations are approximately the same (as are the diagonal energies). The principal difference between the two models is that the t_{2g} and e_g bands are separated for the second model but overlap for the first.

The dashed curves in Fig. 6 are the energy bands for $(pp\sigma) = (pp\pi) = 0$. Again, one sees that the conduction bands are essentially unaffected by this approximation.

IV. SURFACE STATES OF PEROVSKITES

In this section we address the problem of determining the nature of surface states on the d-band perovskites. We formulate the general problem and then derive analytical solutions for the model in which oxygen-oxygen interactions are neglected. The behavior of the surface states depends principally upon changes in the electrostatic Madelung potentials and crystal field symmetry at and near the surface. The effects of changes in lattice spacing and small rotations of the oxygen–B-metal ion bond are also investigated. Graphical results for the various surface states produced are presented for the approximate model. The results for the conduction surface bands are expected to be more exact than those for the valence surface bands since as we have seen the conduction bands depend only very weakly on the p-p interactions. The qualitative features of the valence surface states are correct but the dispersion produced by $(pp\sigma)$ and $(pp\pi)$ is absent.

A. Spatial Variations in Madelung Potentials near a Surface

The spatial variations in the electrostatic potentials of complex cubic crystals have been discussed in detail by Kraut, Wolfram, and Hall.[57] The results of the procedure are summarized in Table II. We present here only the procedure. For the perovskite structure, there are two different types of (001) surfaces as illustrated in Fig. 7. The type-I (001) surface has B and oxygen ions exposed while for the type-II surface, the A and oxygen ions are exposed. The procedure used in obtaining Table II assumes charge neutrality on each plane parallel to the surface. This requirement leads to the condition that the effective charges must be in the proportion $q(A) : q(B) : q(O) = 2 : 4 : 2$. Clearly, for $KTaO_3$, where the formal charge ratios are 1 : 5 : 2, this restriction must be removed. For this crystal alternate (001) surfaces would have net charges. Reconstruction of the surface and the build-up of space charge near the surface would be expected. The use of the neutralized plane potentials described here leads to a situation in which the background charges do not cancel on an atomic scale but do on a macroscopic scale. This gives a model in which

TABLE II. Madelung potentials as functions of depth below type-I and type-II (001) surfaces on ABO_3 crystals.

$v_M^{(A)}$(Bulk)	= 5.3872	$v_M^{(B)}$(Bulk)	= 12.3775
$v_{M\,II}^{(A)}(0)$	= 4.9783	$v_{M\,I}^{(B)}(0)$	= 11.7045
$v_{M\,I}^{(A)}(\frac{1}{2})$	= 5.4159	$v_{M\,II}^{(B)}(\frac{1}{2})$	= 12.4092
$v_{M\,II}^{(A)}(1)$	= 5.3860	$v_{M\,I}^{(B)}(1)$	= 12.3762
$v_{M\,I}^{(A)}(\frac{3}{2})$	= 5.3873	$v_{M\,II}^{(B)}(\frac{3}{2})$	= 12.3775
$v_{M\,II}^{(A)}(2)$	= 5.3872	$v_{M\,I}^{(B)}(2)$	= 12.3775
$v_M^{(O)}$(Bulk)	= −6.4559	($e^2/2a$ = 3.6875, $SrTiO_3$)	
$v_{M\,I}^{(O)}(0)$	= −6.4590	$v_{M\,II}^{(O)}(0)$	= −5.5127
$v_{M\,I}^{(O)}(\frac{1}{2})$	= −6.4845	$v_{M\,II}^{(O)}(\frac{1}{2})$	= −6.4590
$v_{M\,I}^{(O)}(1)$	= −6.4559	$v_{M\,II}^{(O)}(1)$	= −6.4546
$v_{M\,I}^{(O)}(\frac{3}{2})$	= −6.4560	$v_{M\,II}^{(O)}(\frac{3}{2})$	= −6.4559
$v_{M\,I}^{(O)}(2)$	= −6.4559	$v_{M\,II}^{(O)}(2)$	= −6.4559

space charge of opposite sign is accumulated on alternate layers. The problem of surface reconstruction and charged surfaces will not be dealt with in this paper.

For the (2, 4, 2) perovskites, the reduced potentials at and near the surface given in Table II, Madelung potentials $v_{M\,I}^{(\alpha)}$ and $v_{M\,II}^{(\alpha)}$ are obtained from the numbers listed in Table II by multiplying by $(e^2/2a)[q(O)/2]$.

Inspection of Table II shows that the potentials of the A and oxygen ions are reduced in magnitude by 8% and 15%, respectively, on a type-II surface. One layer in from the type-II surface, the B ion has a potential increased by only 0.2%. On the type-I surface, the B and oxygen potentials are reduced by 5% and 0.05% while on the next layer, the A-ion potential is increased by 0.5%.

The potentials approach their bulk values one layer in from the surface. A somewhat surprising feature is the fact that the oxygen potential on a type-I surface is very nearly equal to its bulk value.

The effects of vacancies and extra atoms on the surface or impurities can be included in the potentials by adding or subtracting individual Coulomb contributions to the potentials. The effect of a rough surface can be simulated in this manner. Since additional atoms or vacancies occur in a random fashion, a distribution of surface potentials will result. The values of the surface potentials obtained here will be used as an indicator of the magnitudes expected.

For $SrTiO_3$, using $q(O) = 1.6314$, we find that on a type-I surface, the Madelung potential is decreased by 2 eV at the Ti site and decreased by 0.01 eV at the oxygen site. For the type-II surface, the potential at the Ti site one layer in is increased by 0.07 eV, while on the surface, the oxygen potential is increased by 2.8 eV. Irregularities, vacancies, and impurities can lead to a distribution of potentials but these values are representative of the orders of magnitude expected.

B. Electrostatic Splitting at (001) Surface

The symmetry of the crystal field at lattice sites at and near the surface is lower than in the interior of the crystal. This lower symmetry leads to additional splitting of the d and p orbitals. To determine the nature of this splitting, let us consider the nearest-neighbor ligands. On the type-I surface, the B-metal ion is surrounded by four nearest-neighbor coplanar surface oxygen anions and a single oxygen at $z = +a$. The geometry is illustrated in Fig. 7. Following Sugano *et al.*,[53] the potential is expanded in terms of Legendre polynomials to obtain

$$f^{I}(B;\ r) = -\frac{q(O)e^2r^2}{a^3}\,C_0^{(2)} + \frac{Ze^2r^4q(O)}{a^5} \times \left[\tfrac{5}{2}\,C_0^{(4)} + \tfrac{7}{2}\sqrt{\tfrac{5}{14}}\,(C_4^{(4)} + C_{-4}^{(4)})\right], \quad (15)$$

$$C_m^{(K)}(\theta\phi) = \left(\frac{4\pi}{2k+1}\right)^{1/2} Y_{km}(\theta\phi),$$

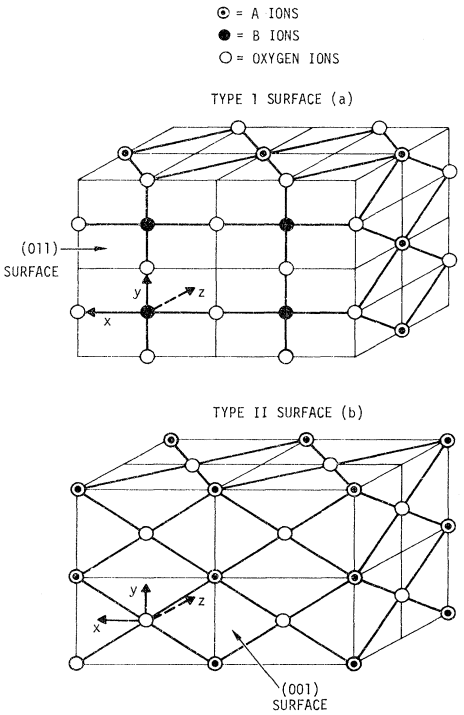

FIG. 7. Schematic of the two types of (001) surfaces of the ABO_3 perovskite structure and the coordinate systems used.

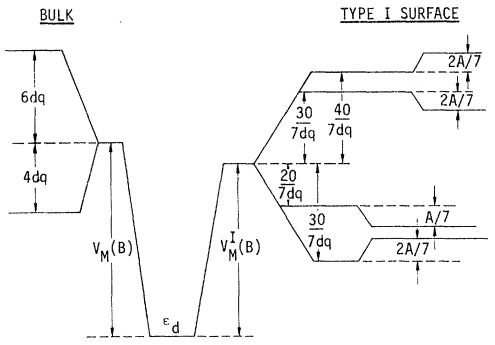

FIG. 8. Energy-level diagram for the B-metal ion in the ABO_3 perovskite crystal. The left-hand side shows the splittings in the bulk and the right-hand side shows those for a type-I surface. The diagonal matrix elements corresponding to these levels are also given.

where $Y_{km}(\theta\phi)$ are the spherical harmonic functions. Terms involving $C_m^{(1)}$ and $C_m^{(3)}$ and $C_m^{(K)}$ $(K>4)$ do not contribute to the d-orbital splitting and have been omitted from Eqs. (15). The energy shifts due to this potential may be evaluated using atomic orbitals. The results are

$$\begin{aligned} &v_{yz}^{\mathrm{I}}(B)=v_\xi=-\tfrac{1}{7}Aq(\mathrm{O})-\tfrac{20}{7}dq(\mathrm{O}),\\ &v_{xz}^{\mathrm{I}}(B)=v_\eta=v_\xi,\\ &v_{xy}^{\mathrm{I}}(B)=v_\zeta=\tfrac{2}{7}Aq(\mathrm{O})-\tfrac{30}{7}dq(\mathrm{O}),\\ &v_{x^2-y^2}^{\mathrm{I}}(B)=v_\nu=\tfrac{2}{7}Aq(\mathrm{O})+\tfrac{40}{7}dq(\mathrm{O}),\\ &v_{3z^2-r^2}^{\mathrm{I}}(B)=v_\mu=-\tfrac{2}{7}Aq(\mathrm{O})+\tfrac{30}{7}dq(\mathrm{O}) \end{aligned} \tag{16}$$

where, for our model

$$\begin{aligned} &A=(e^2/a^3)\langle r^2\rangle,\\ &d=(35/4a^5)e^2[(2/105)\langle r^4\rangle],\\ &\langle r^n\rangle=\int_0^\infty dr\,|rR_d(r)|^2 r^n. \end{aligned} \tag{17}$$

The quantity d is frequently denoted by D. However, the full crystal field splitting does not result from this type of model. We reserve the symbol Dq for the molecular-crystal-field-splitting parameter including overlap and covalency effects. This point has been discussed by Sugano *et al.*[53] and also by Mattheiss.[50] In the case of the infinite crystal, the splittings are

$$\begin{aligned} &v_t=v_\xi=v_\eta=v_\zeta=-4dq(\mathrm{O}), && t_{2g}\text{ levels}\\ &v_e=v_\nu=v_\mu=+6dq(\mathrm{O}), && e_g\text{ levels}. \end{aligned} \tag{18}$$

The magnitude of the term A can be calculated from Eq. (17) but such an estimate is unreliable. Recently, paramagnetic-resonance experiments by Müller *et al.*[58] on Ni^{3+} ion-oxygen vacancy pairs indicates that the crystal field of fivefold-coordinated ions is about 8% smaller than that for sixfold coordination. It should be noted that this reduction is of the same order as the reduction in the Madelung potential at the surface. We shall assume that the quantity A is of this order and therefore much smaller than dq in Eq. (16). The d-level splittings for surface atoms are shown schematically in Fig. 8.

In the case of the oxygen orbitals the effective axial crystalline field is of the form

$$f(0;r)=A_1C_0^{(2)}(\theta,\phi)+B_1\tfrac{1}{2}\sqrt{6}\,[C_2^{(2)}(\theta,\phi)+C_{-2}^{(2)}(\theta,\phi)].$$

For the bulk $A_1=|B_1|$ and the splittings are $v_\perp=\frac{2}{5}A_1$, and $v_\parallel=-\frac{4}{5}A_1$. At or near to a surface $A_1\neq|B_1|$ and additional splitting can occur. The degeneracy of the two $p_\perp$ orbitals is removed. The magnitude of the parameters A_1 and B_1 are modified at the surface. If we consider only the nearest-neighbor B-ion contributions to A_1 and B_1, then $A_1^{\mathrm{I}}=B_1^{\mathrm{I}}=A_{\mathrm{Bulk}}$ for a type-I surface and no additional splitting occurs. For the type-II surface $A_1^{\mathrm{II}}=B_1^{\mathrm{II}}=\frac{1}{2}A_{\mathrm{Bulk}}$ and no additional splitting occurs. Additional splitting results from consideration of more distant neighbors. Also, the change in the magnitude of A^{II} relative to the bulk value is not so drastic when more distant-neighbor interactions are included. We shall ignore the additional splitting and assume the change in the magnitude of the axial splitting scales as the change in the oxygen Madelung potential at the surface. According to this scheme, the splittings are essentially unchanged for the type-I surface and are reduced by about 15% on a type-II surface. Similarly, for a type-II surface, the d-orbital splittings are assumed to be unaltered from the bulk values since the B-metal ion is one layer from the surface.

C. Matrix Equation for Surface States

In this section we discuss the LCAO model for a finite crystal. Perturbation in the diagonal matrix elements of ions at or one layer from the surface will be considered. The effect of changes in the lattice spacing and small rotations of the B-metal–oxygen bonds at the surface are included by changing the strength of the p-d interactions. The perturbations included do not change the two-dimensional periodicity.

In constructing the matrix equations, we make use of the two-dimensional periodicity parallel to the surface. The finite crystal extends between the planes $Z=0$ and $Z=2Na$ where N is the number of unit cells (one-half the number of layers) and a is the layer spacing. The basis functions are the two-dimensional Bloch functions. One obtains the matrix equation

$$H(k_\parallel)\psi_s=E(k_\parallel)\psi_s, \tag{19}$$

where H is a $N\times N$ supermatrix of 14×14 matrices, $k_\parallel$ is the two-dimensional wave vector parallel to the surface (in the x-y plane), and ψ_s is an eigenvector with $14N$ components which specify the

amplitudes of the 14 orbitals on each plane parallel to the surface. For the same approximation used in deriving the bulk bands [including $(pp\sigma)$ and $(pp\pi)$], the matrix $H(k_{\parallel})$ is a nearest-neighbor supermatrix. The diagonal blocks $D(Z_i)$ are 14×14 matrices corresponding to interactions of atoms in unit cells parallel to the surface. The off diagonals connect atoms with unit cells whose origins are displaced by $2a$ in the $\pm Z$ direction. Interactions between a cell at Z and one at $Z-2a$ are represented by $B(Z_i,\ Z_i-2a)$ and $B^+(Z_i,\ Z_i+2a) = B(Z,\ Z_i-2a)$. The form of the matrix is

$$H(K_{\parallel})=\begin{pmatrix} D'B & & & & \\ B^+DB & & & & \\ & B^+DB & & & \\ & & \ddots & & \\ & & & B^+D' \end{pmatrix}. \tag{20}$$

Perturbations due to changes in the electrostatic potentials, bond angles, and lattice spacing at the surface are included in D' and all other $D(Z_i)=D$ are the same. Equation (20) can be solved numerically for the eigenvalues and eigenvectors by considering only a few layers. Such a procedure does not give a great amount of insight into physical features of the surface energy bands unless accompanied by an analytical model. In this work we are concerned primarily with extracting the qualitative features of the surface states.

D. Qualitative Features of Surface Energy Bands

In this section we derive analytical expressions for the surface energy bands for a semi-infinite solid. By neglecting the $(pp\pi)$ and $(pp\sigma)$ interactions, we can find exact solutions for the surface states including the perturbations in the electrostatic potentials and changes in the transfer integrals at the surface. The model is also exactly soluable for a finite slab using the same procedure. The results, however, indicate that the surface states are highly localized at the surface so that no significant effects are neglected by considering only the semi-infinite slab.

For $(pp\sigma)=(pp\pi)=0$, Eq. (20) can be block diagonalized in the same fashion as described in Sec. III. The reduced surface-matrix problem then consists of three 3×3 supermatrices giving the t_{2g} surface states, and the upper valence-band surface states, and a 5×5 supermatrix which gives the e_g conduction-band surface states and the lower valence-band surface states. We now consider the 3×3 supermatrix equation which has the form

$$\begin{pmatrix} (D'_{\alpha\beta}-E)B_{\alpha\beta} & & \\ B^+_{\alpha\beta}(D_{\alpha\beta}-E)_{\alpha\beta} & & \\ & {}_{\alpha\beta}(D_{\alpha\beta}-E) & \\ & & \ddots \end{pmatrix}\begin{pmatrix} \vec{S}_1 \\ \vec{S}_2 \\ \vec{S}_3 \\ \vdots \end{pmatrix}=0, \tag{21}$$

$$\vec{S}_n=\begin{pmatrix} s_n^{(1)} \\ s_n^{(2)} \\ s_n^{(3)} \end{pmatrix}, \tag{22}$$

where for $\alpha=y$, $\beta=z$,

$$D_{yz}=\begin{pmatrix} E_t-E & (pd\pi) & 2iS_y(pd\pi) \\ (pd\pi) & E_\perp-E & 0 \\ -2iS_y(pd\pi) & 0 & E_\perp-E \end{pmatrix}. \tag{23}$$

B_{yz} has only a single nonzero element, $(B_{yz})_{12} = -(pd\pi)=(B^+_{yz})_{21}$. The initial matrix D'_{yz} has the form

$$D'_{yz}=\begin{pmatrix} E'_t-E & (pd\pi)' & 2iSy(pd\pi)'' \\ (pd\pi)' & E_\perp-E & 0 \\ -2iS_y(pd\pi)'' & 0 & E'_\perp-E \end{pmatrix}. \tag{24}$$

The perturbed energies E'_t and $E'_\perp$ differ from the bulk values because of changes in the Madelung potentials and the electrostatic splitting. The 2, 2 element corresponds to a p_y orbital one layer in from the surface so that the electrostatic potentials are essentially unchanged. Therefore, we assume no perturbation in this element. The 1, 2 and 2, 1 elements $(pd\pi)'$ correspond to π transfer integrals between the p_y orbitals one layer from the surface and the d_{yz} orbitals on the surface. It is quite likely that the spacing between the first two layers is slightly modified. For example, Tong and Maradudin[59] found an expansion of about 0.5% from the bulk lattice spacing at the surface of a NaCl lattice. Such an expansion would act to reduce the $(pd\pi)$ interaction since the transfer integrals decrease exponentially with increasing separation of the ions. The 1, 3 and 3, 1 elements represent π transfer between a p_z orbital and a d_{yz} orbital on the surface. Changes in the bond angle are represented by $(pd\pi)''$. The situation is shown schematically in Fig. 9. The quantity $(pd\pi)''$ can be

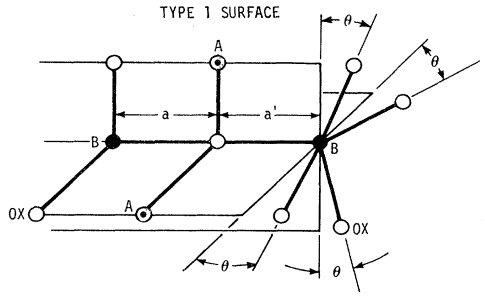

FIG. 9. Schematic showing the increase in the lattice spacing from a to a' and small rotations of the oxygen–B-metal bond at a (001) type-I surface.

written[35] as $\sin^2\theta\cos\theta(pd\sigma)+\cos\theta(1-2\sin^2\theta)(pd\pi)$. Since $(pd\sigma)$ is greater than $(pd\pi)$, it follows that rotation of the bonds leads to an increased transfer integral. The surface perturbations considered here do not destroy the two-dimensional periodicity of the crystal. The remaining elements of D'_{yz} are equal to those of D_{yz}. The vectors $\vec{s}_n$ give the amplitudes of the wave functions in the a cell n layers in from the surface. The components $s_n^{(1)}$, $s_n^{(2)}$, and $S_n^{(3)}$ correspond to the amplitudes of the $d_{yz}(B)$, $p_y^{(3)}$, and $p_z^{(2)}$ in the nth unit cell. For the type-I surface, the diagonal energy corresponding to $p_y^{(3)}$ is unmodified. According to Table II, the energy of $p_z^{(2)}$ should also be unchanged. We include the possibility of changes in the energy of this orbital since surface irregularities are likely to change the surface potentials.

If we write out the equations of Eq. (21) we find that

$$\begin{aligned}&(\epsilon_t'-\epsilon)s_1(1)+\epsilon' s_1(2)+2i\epsilon'' S_y s_1(3)=0\,,\\&(\epsilon_\perp-\epsilon)s_1(2)+\epsilon' s_1(1)-s_2(1)=0\,,\\&(\epsilon'-\epsilon)s_1(3)-2i\epsilon'' S_y s_1(1)=0\,,\end{aligned}\tag{25}$$

and for $n>1$

$$\begin{aligned}&(\epsilon_t-\epsilon)s_n(1)+s_n(2)-s_{n-1}(2)+2iS_y s_n(3)=0\,,\\&(\epsilon_\perp-\epsilon)s_n(2)+s_n(1)-s_{n+1}(1)=0\,,\\&(\epsilon_\perp-\epsilon)s_n(3)-2iS_y s_n(1)=0\,.\end{aligned}\tag{26}$$

In Eqs. (25) and (26), $\epsilon_\perp=E_\perp/(pd\pi)$, $\epsilon=E/(pd\pi)$, $\epsilon'=(pd\pi')/(pd\pi)$, and $\epsilon''=(pd\pi)''/(pd\pi)$. From Eq. (26), we can express all amplitudes in terms of $s_n(1)$ (for $n\geq 2$) giving

$$s_n(3)=\frac{2iS_y}{\epsilon_\perp-\epsilon}\,s_n(1)\,,\qquad s_n(2)=\frac{s_{n+1}(1)-s_n(1)}{\epsilon_\perp-\epsilon}\,.\tag{27a}$$

The equations for $s_1(1)$ give

$$s_1(3)=\frac{2iS_y s_1(1)\epsilon''}{\epsilon_\perp'-\epsilon}\,,\qquad s_1(2)=\frac{s_2(1)-s_1(1)\epsilon'}{\epsilon_\perp-\epsilon}\,;\tag{27b}$$

then

$$[(\epsilon_\perp-\epsilon)(\epsilon_t-\epsilon)-(2+4S_y^2)]s_n(1)+s_{n+1}(1)+s_{n-1}(1)=0\,,\tag{28a}$$

$$[(\epsilon_\perp-\epsilon)(\epsilon_t-\epsilon)-(2+4S_y^2)+\Delta p]+s_2(1)=0\,,\tag{28b}$$

$$\Delta p=(\Delta\epsilon_t+\epsilon_t-\epsilon)(\epsilon_\perp-\epsilon)-(\epsilon')^2-4(\epsilon'')^2S_y^2\,\frac{\epsilon_\perp-\epsilon}{\Delta\epsilon_\perp+\epsilon_\perp-\epsilon}-(\epsilon_t-\epsilon)(\epsilon_\perp-\epsilon)+(2+4S_y^2)\,,\tag{28c}$$

$$\Delta\epsilon_t=\epsilon_t'-\epsilon_t\,,\quad \Delta\epsilon_\perp=\epsilon_\perp'-\epsilon_\perp\,.$$

Simultaneous solution of Eqs. (28a) and (28b) yields the surface energy bands and wave functions. If we define

$$(\epsilon_t-\epsilon)(\epsilon_p-\epsilon)-(2+4S_y^2)=-2\cos\theta\,,\tag{29}$$

then Eqs. (27) and (28) may be written

$$(M+\Delta M)\vec{S}(1)=0\,,\tag{30}$$

where

$$M=\begin{pmatrix}-e^{-i\theta},\ 1,\ 0,\ 0,\ 0,\ 0,\ \dots\\ 1,\ -2\cos\theta,\ 1,\ 0,\ 0,\ 0,\ \dots\\ 0,\ 1,\ -2\cos\theta,\ 1,\ 0,\ 0,\ \dots\\ \ddots\quad\ddots\quad\ddots\end{pmatrix}\,,\tag{31}$$

$$\begin{aligned}&\Delta M_{11}=\Delta p-e^{i\theta}\,,\\&\Delta M_{ij}=0\ \text{ otherwise}\,,\end{aligned}\tag{32}$$

$$\vec{S}(1)=\begin{pmatrix}s_1(1)\\ s_2(1)\\ s_3(1)\\ \vdots\end{pmatrix}\,.\tag{33}$$

The surface energy bands are then determined by

$$|I+G\Delta M|=0\,,\tag{34}$$

where $G=M^{-1}$ and

$$G_{ll'}=\frac{e^{i\theta}|l-l'|}{2i\sin\theta}\,.\tag{35}$$

That $M^{-1}G=I$ is easily demonstrated by direct matrix multiplication. Since ΔM has only a single nonzero element, Eq. (34) reduces to simply

$$\Delta p=e^{-i\theta}\,.\tag{36}$$

Then, using the definition of $\cos\theta$, we obtain the eigenvalue condition

$$\Delta p+(1/\Delta p)=(2+4S_y^2)-(\epsilon_t-\epsilon)(\epsilon_\perp-\epsilon)\,.\tag{37}$$

[Note that the surface energy can be obtained directly from Eq. (37) in the special case that Δp is independent of ϵ.] The eigenstates are obtained from the relation $(I+G\Delta M)\vec{S}(1)=0$, which yields

$$s_l(1)=-G_{1l}(\Delta p-e^{i\theta})s_1(1)\,.\tag{38}$$

For $l=1$, we obtain the eigenvalue equation, Eq. (36). Making use of this relation, we find that

$$\frac{s_l(1)}{s_1(1)}=e^{i|1-l|\theta}\,.\tag{39}$$

For a surface state we require that $\mathrm{Im}\,\theta>0$. Since Δp is real [Eq. (28)], Eq. (36) requires that $\theta=i\alpha$ for $\Delta p>0$ and $\theta=\pi+i\beta$ for $\Delta p<0$, with α and β real positive coefficients. Thus for $\Delta p>0$

$$\frac{s_l(1)}{s_1(1)}=e^{-|1-l|\alpha}\,,\tag{40}$$

and for $\Delta p<0$

$$\frac{s_l(1)}{s_1(1)}=(-1)^{|1-l|}e^{-|1-l|\beta}\,.\tag{41}$$

We note that since $\Delta p=e^{\alpha}$ or $-e^{\beta}$, then $|\Delta p|>1$ for

a solution to exist. Returning to the definition of $\cos\theta$, we find that since $\cosh\alpha \geq 1$ (for $\Delta p > 0$) that

$$(\epsilon_t - \epsilon)(\epsilon_\perp - \epsilon) - (2 + 4S_y^2) \leq -2 . \quad (42)$$

When the equality holds, the energy is given by

$$\epsilon = \tfrac{1}{2}(\epsilon_t + \epsilon_p) \pm \{[\tfrac{1}{2}(\epsilon_t - \epsilon_p)]^2 + 4 + 4S_y^2\}^{1/2} \quad (43)$$

and when the inequality holds, ϵ lies between these two bands. Referring back to Eq. (9), we see that Eq. (43) describes the bulk t_{2g} and upper valence bands for $K_z = 0$. We refer to these as the conduction, and valence-band edges. Thus, surface states for $\Delta p > 0$ lie in the energy gap of the bulk bands between the band edges.

For $\Delta p < 1$, $\cos\theta = -\cosh\beta$ and we obtain the inequality

$$(\epsilon_t - \epsilon)(\epsilon_\perp - \epsilon) - (2 + 4S_y^2) \geq 2 . \quad (44)$$

The equality gives

$$\epsilon = \tfrac{1}{2}(\epsilon_t + \epsilon_\perp) \pm \{[\tfrac{1}{2}(\epsilon_t - \epsilon_\perp)]^2 + 4 + 4S_y^2\}^{1/2} . \quad (45)$$

Equation (45) describes the bottom of the valence band and the top of the conduction band for $K_z a = \frac{1}{2}\pi$. The inequality is satisfied for energies above the conduction band or below the valence band. Thus there are no solutions within the bulk bands (except for special conditions described later).

Equation (37) for the surface energy gives a fifth-order polynomial equation. A root of this polynomial is a solution only when $|\Delta p| > 1$ for that root. Multiple surface branches generally exist. Their number and dispersion depends upon the perturbations. If all perturbations vanish, then $\Delta p = 1$ [Eq. (28)] and no surface branch exists.

Consider the simple case for which the only nonvanishing perturbation is $\Delta\epsilon_t$. For this situation, the eigenvalue condition is

$$[\Delta\epsilon_t(\epsilon_\perp - \epsilon) + 1]^2 + 1 + [(\epsilon_\perp - \epsilon)(\epsilon_t - \epsilon) - (2 + 4S_y^2)] \times [\Delta\epsilon_t(\epsilon_\perp - \epsilon) + 1] = 0 . \quad (46)$$

For small $\Delta\epsilon_t < 0$, a surface band below the conduction band in the gap is formed with energy

$$\epsilon = \epsilon_B + a\Delta\epsilon_t^2 + b\Delta\epsilon_t^3 + c\Delta\epsilon_t^4 ,$$
$$a = \frac{(\epsilon_\perp - \epsilon_B)^2}{\epsilon_\perp + \epsilon_t - 2\epsilon_B} , \quad (47)$$
$$b = -a(\epsilon_\perp - \epsilon_B) ,$$
$$c = \frac{a^2 - 2a(\epsilon_\perp - \epsilon_B)}{\epsilon_\perp + \epsilon_t - 2\epsilon_B} + (\epsilon_\perp - \epsilon_B)^2 a ,$$

where ϵ_B is the conduction-band-edge energy given by Eq. (43). It is clear that the surface band will be separated from the conduction band by an amount less than $\Delta\epsilon_t$ for small $\Delta\epsilon_t$. This feature is generally true. At the point Γ in the Brillouin zone, Eq. (47) reduces to

$$\epsilon = \epsilon_t + (\epsilon_\perp - \epsilon_t)(\Delta\epsilon_t^2 - \Delta\epsilon_t^4) - (\epsilon_\perp - \epsilon_t)^2(\Delta\epsilon_t^3 - \Delta\epsilon_t^4) .$$

The approximation Eq. (47) is valid only for $(\epsilon_\perp - \epsilon_t)\epsilon_t \ll 1$. For larger $\Delta\epsilon_t$, the energy separation becomes comparable to $\Delta\epsilon_t$ but is less. As the perturbations increase in strength, additional surface bands appear. Some additional bands first occur near the edge of the zone (point X) and are truncated at some value of $k_\parallel$. For example, in Fig. 10(a), the surface band below the valence band for $\Delta\epsilon_t = -2$ eV is truncated at the point indicated by the arrow while for $\Delta\epsilon_t = -4$ eV, it exists over the entire zone. The spatial extent of a surface state is easily obtained from Eqs. (36) and (39). Since $\Delta p = e^{-i\theta}$, it follows that

$$\frac{s_l(1)}{s_1(1)} = \left(\frac{1}{\Delta p}\right)^{|1-l|} . \quad (48)$$

Using Eqs. (27a) and (27b), the amplitudes of $s_l(2)$ and $s_l(3)$ are easily found. It is clear from Eq. (48) that the surface-state localization increases with Δp (for $|\Delta p| > 1$). The separation of a surface band from the bulk band also increases with increasing perturbation. For the case discussed previously (small $\Delta\epsilon_t$), one can deduce that

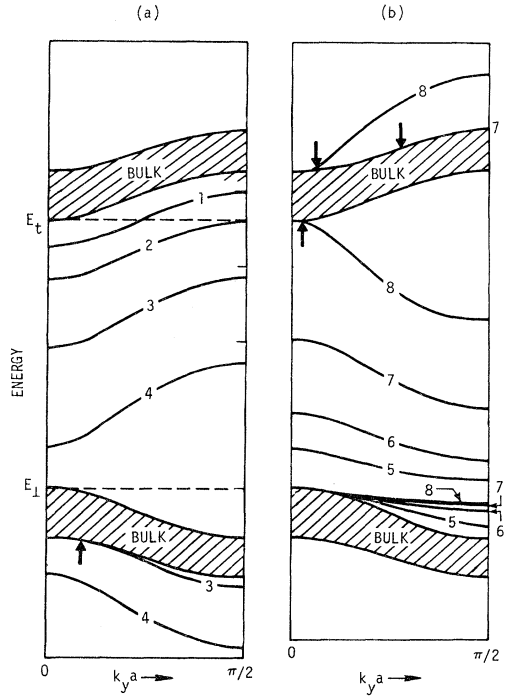

FIG. 10. Surface states formed at a type-I (001) surface of $SrTiO_3$ for various values of the surface perturbations. The arrows indicate the point at which a surface band is truncated. The calculations use the parameters of Fig. 5. The surface perturbations are: (1) $\Delta E_t = -0.5$, $\Delta E_\perp = 0.0$; (2) -1.0, 0.0; (3) -2.0, 0.0; (4) -4.0, 0.0; (5) 0.0, 0.5; (6) 0.0, 1.0; (7) 0.0, 2.0; and (8) 0.0, 4.0.

$$\frac{s_l(1)}{s_1(1)} \approx \left(\frac{1}{1+(\epsilon_\perp-\epsilon_B)\Delta\epsilon_t}\right)^{|1-l|}. \quad (49)$$

For larger values ($\Delta\epsilon_t \leq -1$), the surface band is separated from the bulk band by an energy comparable to $\Delta\epsilon_t$.

A series of surface bands for different perturbations are illustrated in Figs. 10 and 11. These calculations were made using the parameters employed for Fig. 5 with $(pp\sigma)=(pp\pi)=0$.

The surface bands produced when the parameters used for Fig. 6 are employed are very similar and therefore we shall not reproduce them here. Clearly, a variety of surface bands can be produced using the various perturbations $\Delta\epsilon_t$, $\Delta\epsilon_\perp$, ϵ', and ϵ''. An increase in the lattice spacing at the surface leads to a decrease in $\epsilon'(\epsilon'<1)$. This effect produces conduction and valence surface bands. With only ϵ' as a perturbation, the surface bands are described by

$$\epsilon = \tfrac{1}{2}(\epsilon_t+\epsilon_\perp) \pm \{[\tfrac{1}{2}(\epsilon_\perp-\epsilon_t)]^2+(\epsilon')^2 - [2-(\epsilon')^2]^{-1}+4S_y^2\}^{1/2} \text{ for } \epsilon'<1. \quad (50)$$

This band lies in the energy gap and follows the conduction-(valence) band edge approximately. Changes in ϵ'' result from rotation of the oxygen–B-metal ion band. Small rotations result in an increase in the p-d interaction. Study of Eq. (28c) shows that this effect is opposed to the effect of lowering of the electrostatic potentials of the oxygen atom on the surface. Solutions containing this effect can easily be studied using Eq. (37). No further discussion of this perturbation will be given here. We have yet to consider the other surface states corresponding to $\alpha\beta=xy$ which are admixtures of d_{xy}, $p_y^{(1)}$, and $p_x^{(2)}$. In the approximation $(pp\pi)=(pp\sigma)=0$ there is no coupling between these orbitals on different layers parallel to the surface. The surface layer states are therefore independent of the other layers. The solutions are given by

$$\epsilon=\epsilon_t', \quad \epsilon = \tfrac{1}{2}(\epsilon_\perp'+\epsilon_t') \pm \{[\tfrac{1}{2}(\epsilon_\perp'-\epsilon_t')]^2+4(\epsilon'')^2(S_x^2+S_y^2)\}^{1/2}. \quad (51)$$

These surface states are confined entirely to the surface layer. They may have energies, depending on the perturbations, which lie in the bulk continuum of states. If there are no perturbations, then the dispersion is identical to the bulk band edge. Since the transfer integrals $(pp\pi)$ and $(pp\sigma)$ are small, inclusion of these terms will not destroy these features. Therefore, virtual surface states could exist within the bulk bands. However, one expects on the basis of the electrostatic energies that the perturbations will push these surface bands into the energy-gap region.

Next consider the states for $\alpha\beta=xz$. The problem is clearly the same as for the case $\alpha\beta=yz$ and all expressions derived above can be used if S_x is substituted for S_y.

1. Type-II Surface Bands

The discussion of surface states to this point has been for the type-I surface in which the B-metal ion is on the surface. The nature of the surface states is modified in the surface is a type-II surface. The surface-state–matrix problem is still described by Eq. (20). The matrix elements of D_{yz} are given by Eq. (23) with the following changes:

$$(D_{yz})_{12}=(D_{yz})_{21}=-(pd\pi). \quad (52)$$

For the initial matrix, D'_{yz} differs in that

$$(D'_{yz})_{12}=(D'_{yz})_{12}=-(pd\pi)', \quad (D_{yz})_{22}=\epsilon_t'-\epsilon. \quad (53)$$

Perturbations in the energies of the d_{yz} and $p_z^{(2)}$ are negligible since these ions are not on the surface for the type-II case. The only nonvanishing element of B is $B_{12}=(pd\pi)$. Proceeding as in the previous case, we find the eigenvalue condition of the form given by Eq. (37), where now

$$\Delta p = 1-\left|\frac{(pd\pi)'}{(pd\pi)}\right|^2\left(\frac{\epsilon_\perp-\epsilon}{\epsilon_\perp'-\epsilon}\right). \quad (54)$$

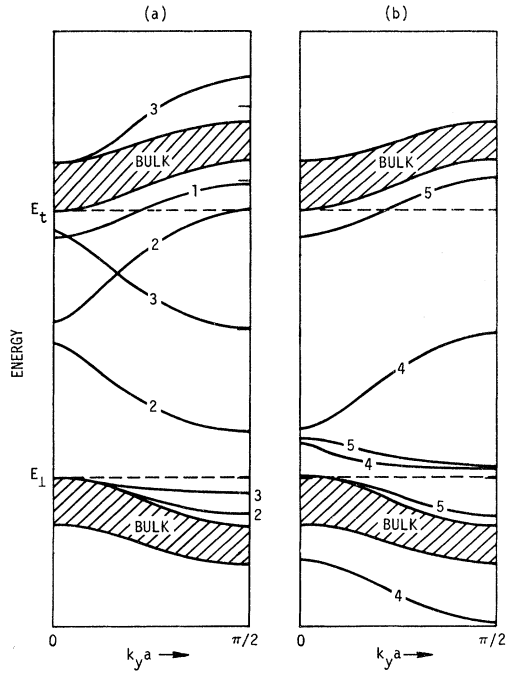

FIG. 11. Surface bands formed at a type-I (001) surface of $SrTiO_3$ for various surface perturbations. The calculations use the parameters of Fig. 5. The surface perturbations are (1) $\Delta E_t=0.5$, $\Delta E_\perp=0.0$; (2) 2.0, 2.0; (3) −0.5, 4.0; (4) −4.0, 0.5; and (5); −0.5, 0.5.

All the formal results [Eqs. (37)–(45) and (48)] previously discussed still apply with Δp given by Eq. (54). If $(pd\pi)' \equiv (pd\pi)$ and $\epsilon_\perp' \equiv \epsilon_\perp$, then no surface solutions occur. However, because of the denominator in Δp, an arbitrarily small perturbation produces an arbitrarily large Δp when $\epsilon \to \epsilon_\perp'$ and consequently a surface branch derived from the flat valence band at $\epsilon = \epsilon_\perp$ occurs at an energy $\epsilon \geq \epsilon_\perp$. If both perturbations are small, we can find the surface-state energy. We write

$$\left|\frac{(pd\pi)'}{(pd\pi)}\right|^2 = 1 - \delta\,, \quad \epsilon = \epsilon_\perp + a\Delta\epsilon_\perp\,, \quad \Delta\epsilon_\perp = \epsilon_\perp' - \epsilon_\perp\,, \tag{55}$$

and obtain $\Delta p = (1 - \delta a)/(1 - a) \approx (1 - a)^{-1}$ for $\delta \ll 1$. Clearly, a must be positive for a solution since Δp must be greater than 1. Using Eq. (37) we find

$$\begin{aligned} a &= 2S_y^2[(1 + S_y^2)^{1/2} - 1]\,, \\ \epsilon &= \epsilon_\perp + 2S_y^2[(1 + S_y^2)^{1/2} - 1]\Delta\epsilon_\perp\,. \end{aligned} \tag{56}$$

This surface branch lies in the energy-gap region and has very little dispersion for $\Delta\epsilon_\perp$ small. We also note that the branch has an upward curvature whereas the valence band has downward curvature. This feature persists even for larger values of $\Delta\epsilon_\perp$ although Eq. (56) is valid only for $\Delta\epsilon_\perp \ll 1$. A series of branches for different values of $\Delta\epsilon_\perp$ with $(pd\pi)' = (pd\pi)$ are shown in Fig. 12. The $(pp\pi)$ and $(pp\sigma)$ interactions will alter these surface branches considerably. These interactions produce dispersion and remove some of the degeneracies among the valence bands.

The $\alpha\beta = xz$ states on the type-II surface have the same behavior as the $\alpha\beta = yz$ states except that S_y is replaced by S_x. The $\alpha\beta = xy$ states are again two-dimensional solutions. Layers parallel to the surface are decoupled. The surface oxygens do not participate in these states when $(pp\pi) = (pp\sigma) = 0$.

2. e_g Surface States

The e_g bulk and surface conduction bands and the lower bulk and surface valence bands are decoupled from the bulk and surface t_{2g} and upper valence bands in the approximation we are using here. The matrix problem for the surface bands can also be expressed as $[H(k_\parallel) - E]\psi_s = 0$ with $H(k_\parallel)$ having the form given by Eq. (20). In this case, the matrices D and B are 5×5 matrices. The same technique used for the t_{2g} states can be applied. The solutions are admixutres of the orbitals $d_{3z^2-r^2}$, $d_{x^2-y^2}$, $p_z^{(1)}$, $p_y^{(2)}$, and $p_x^{(3)}$. The algebra is quite a bit more complicated but one can derive an eigenvalue equation of the form

$$\Delta p + (1/\Delta p) - 2\cos\psi = 0\,. \tag{57}$$

In Eq. (57),

$$2\cos\psi = 2 - \frac{(x - 4\sigma^2 S_x^2)(x - 6\sigma^2 S_y^2) + 2\sigma^2 S_y^2 (x - 6\sigma^2 S_z^2)}{\sigma^2[x - 3\sigma^2(S_x^2 + S_y^2)]}\,, \tag{58}$$

where $x = (E_e - E)(E_\parallel - E)$ and $\sigma = (pd\sigma)$. The parameter Δp contains the perturbations due to electrostatic effects and changes in transfer integrals. Surface states produces below the e_g conduction band can lie in the narrow gap between the e_g and t_{2g} conduction bands if it exists (Fig. 6) or in the t_{2g} bulk bands. Surface bands produced above the lower valence bands lie in the upper bulk valence bands. If the $(pp\pi)$ and $(pp\sigma)$ integrals are included, these surface states are not decoupled from the bulk states. The coupling is weak for the conduction e_g surface bands, and it is probably meaningful to consider them as virtual surface states. In order to determine the lifetime of these states, it is necessary to include the p-p interactions. These questions will be considered in a subsequent paper.

V. SUMMARY AND CONCLUSIONS

In the preceding sections, we have investigated a simple LCAO model for the bulk and surface energy bands of d-band cubic perovskite crystals of which $SrTiO_3$, $BaTiO_3$, $BaZrO_3$, and $KTaO_3$ are examples. The main emphasis was in establishing the qualitative features in terms of the largest energies.

An LCAO model of the type employed by Kahn and Leyendecker was used. The diagonal matrix elements were estimated by using the approach of Seitz for ionic crystals. Two approximate band structures of $SrTiO_3$ were obtained. The first was obtained utilizing the transfer integrals of Kahn and Leyendecker and Switendick together with the ionization potential of Ti^{3+}, the electron affinity of O^-, the observed energy gap, and Madelung poten-

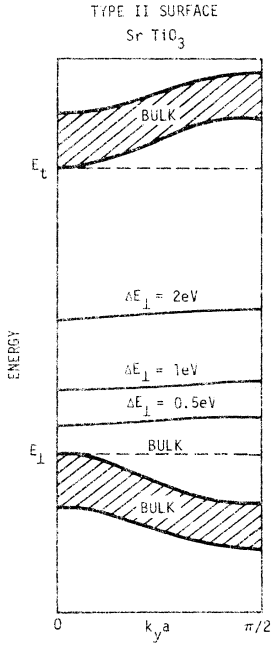

FIG. 12. Surface bands formed at a type-II (001) surface for different perturbations in the oxygen energy. The calculations use the parameters of Fig. 5.

tials. The second band structure was obtained by fitting our model to the more complicated LCAO version of Mattheiss. The two band structures are quite similar. The major difference is the separation of the e_g and t_{2g} conduction bands in the latter model. Exact expressions were derived for the Madelung potentials of cubic crystals with arbitrary charges and numbers of the atoms per unit cell. The effective charges on the ions were varied to produce the proper energy gap at the point Γ in the Brillouin zone. Explicit expressions for the direct gap in terms of the electrostatic energies, free-ion energies, and the $(pp\sigma)$ and $(pp\pi)$ transfer integrals were obtained. For a direct gap of 3.24 eV, an effective oxygen charge of $-1.63|e|$ was obtained for $SrTiO_3$ instead of the full ionic value of $-2|e|$. Analytic expressions for the bulk energy bands and wave functions were derived for the approximation in which the oxygen-oxygen interactions are neglected. The results of this approximation were then compared with the results of the full model. The upper valence bands did not agree as well. The approximation produced several flat (without dispersion) bands which have dispersion when the p-p interactions are included.

The LCAO method was then extended to treat the (001) surface problem. The spatial variations in the Madelung potentials near a surface were obtained. Two types of (001) surfaces occur for the ABO_3 perovskite structure. The type-I surface has oxygen and B-metal ions exposed while the type-II surface has oxygen and A-metal ions. In addition to the changes in the surface Madelung potentials, the changes in the electrostatic splittings of the d and p levels at the surface were investigated. The lower symmetry produces additional splittings. Degeneracy of the two e_g and $p_\perp$ levels is lifted and the three t_{2g} states split into a twofold and singlet level. Changes in the transfer integrals corresponding to changes in the lattice spacing and small rotations in the B-metal–oxygen bonds at the surface were also considered. Analytic expressions for the surface band were obtained neglecting the oxygen-oxygen interactions. The effects of various surface perturbations were studied for both type-I and -II surfaces. For small perturbations, a single band appears in the energy gap. Increasing the perturbations leads to additional bands. Truncated bands which exist only over a portion of the Brillouin zone were found. Analytic expressions for the surface-state wave functions were also derived. In general, the surface states were found to be confined mainly to the first few atomic layers. Special surface states with energies in the bulk continuum were found. The behavior of the e_g and lower valence bands were briefly mentioned.

For the perfect or ideal (001) type-I surface, the Madelung potential is reduced about 2 eV at the Ti site of $SrTiO_3$, while the oxygen potential is essentially unperturbed. Similarly, for a type-II surface, the oxygen potential is increased by about 2 eV while the Ti potential (one layer from the surface) does not change very much. In both cases, surface bands near the center of the band gap are predicted. These surface states can act as efficient recombination centers for both holes and electrons. They would also act as active centers for chemisorption processes.

On the basis of our present analysis, it appears that the d-band perovskites are ideal candidates for the study of d-band surface states and their role in catalysis.

A great deal of additional theoretical work remains to be done. The application of this simple model to other perovskites and in particular to $KTaO_3$ should prove quite interesting. The effects of the p-p interactions on the surface states need to be studied. Since both $(pp\sigma)$ and $(pp\pi)$ are small relative to the other energies considered, their effect can be treated by perturbation theory. The lifetimes of the virtual e_g states can then be determined. The possibility of surface reconstruction presents a more difficult problem but experimental data are lacking at the present time.

In future work, we hope to deal with these problems and the calculation of the chemisorption energy of molecules on the surface of d-band perovskites.

Note added in proof. Recently we have employed the simple analytical model described here to calculate some of the bulk properties of $SrTiO_3$.[60] In this work it is noted that the "two-dimensional" character of the t_{2g} conduction bands [i.e., $E(\vec{k})$ depends only on two components of the wave vector] produces discontinuities and logarithmic singularities in the single-particle Green's function, in the density of states and joint density of states. These features are shown to account for characteristic structure in the optical properties of several perovskites.

ACKNOWLEDGMENTS

The authors wish to thank Dr. W. F. Hall for valuable consultation and Dr. L. F. Mattheiss for making available to us copies of his recent work on $SrTiO_3$ prior to publication.

---

†Work partically supported by the U.S. Air Force Office of Scientific Research Contract No. F44620-72-C-0050.

[1]Z. J. Kiss, Phys. Today, Jan. 1970, p. 42.

[2]B. W. Faughnan, D. L. Staebler, and Z. J. Kiss, *Applied Solid State Science* (Academic, New York, 1971), Vol. 2, pp. 107–172.

[3]B. W. Faughnan and Z. J. Kiss, IEEE J. Quan. Electron. QE-5, 17 (1969); Phys. Rev. Letters 21, 1331

(1968).
[4]B. Faughnan, Phys. Rev. B 4, 3623 (1971).
[5]J. Blanc and D. L. Staebler, Phys. Rev. B (to be published).
[6]J. D. Levine and S. Freeman, Phys. Rev. B 2, 3255 (1970).
[7]F. D. Mango, Advan. Catalysis 20, 291 (1969).
[8]L. F. Mattheiss, Phys. Rev. B 6, 4718 (1972); Phys. Rev. B 6, 4740 (1972).
[9]T. F. Soules, E. J. Kelly, D. M. Vaught, and J. W. Richardson, Phys. Rev. B 6, 1519 (1972); J. W. Richardson, E. J. Kelly, T. F. Soules, and D. M. Vaught, Bull. Am. Phys. Soc. 16, 371 (1971).
[10]A. H. Kahn and A. J. Leyendecker, Phys. Rev. 135, A1321 (1964).
[11]C. E. Moore, *Atomic Energy Levels*, Natl. Bur. Std. Circ. 467 (U.S. GPO, Washington, D.C., 1958), Vol. III.
[12]The electron affinity for adding a single electron O^{2-} is −1.5 eV [C. M. Moser and R. K. Nesbet, Phys. Rev. A 4, 1336 (1971)]. The electron affinity for the adding of two electrons is +7.72 eV [M. P. Tosi, in *Solid State Physics*, edited by F. Seitz and D. Turnbull (Academic, New York, 1964), Vol. 16, pp. 1–120] for the reaction $O^{2-}_{gas} \rightarrow O_{gas} + 2e$ for MgO. The affinity for adding the second electron is taken to be 7.72-(−1.5)=9.22 eV.
[13]F. Seitz, *The Modern Theory of Solids* (McGraw-Hill, New York, 1940), pp. 447–450.
[14]Y. T. Sihvonen, J. Appl. Phys. 38, 4431 (1967).
[15]H. Unoki and T. Sakudo, J. Phys. Soc. Japan 23, 546 (1969).
[16]G. Shirane and Y. Yamado, Phys. Rev. 177, 858 (1969).
[17]J. M. Worlock and P. A. Fleury, Phys. Rev. Letters 19, 1176 (1967).
[18]P. A. Fleury, J. F. Scott, and J. M. Worlock, Phys. Rev. Letters 21, 16 (1968).
[19]H. E. Weaner, J. Phys. Chem. Solids 11, 274 (1959).
[20]V. Dvorak and P. Glogar, Phys. Rev. 143, 334 (1966).
[21]J. F. Schooley, W. R. Hosler, E. Ambler, J. H. Becker, M. L. Cohen, and O. S. Koonce, Phys. Rev. Letters 14, 305 (1965).
[22]L. C. Walters and R. E. Grace, J. Phys. Chem. Solids 28, 239 (1967); 28, 245 (1967).
[23]A. E. Paladino, L. G. Rubin, and J. S. Waugh, J. Phys. Chem. Solids 26, 391 (1965); H. E. Paladino, Bull. Am. Ceram. Soc. 48, 476 (1965).
[24]H. P. R. Frederikse, W. Therber, and W. R. Hosler, Phys. Rev. 134, A442 (1964); Phys. Rev. 161, 822 (1967).
[25]H. Yasunaga and I. Nakado, J. Phys. Soc. Japan 22, 338 (1967); 24, 218 (1968); 24, 1035 (1968).
[26]O. N. Tufte and P. W. Chapman, Phys. Rev. 155, 796 (1967).
[27]W. A. Gandy, Phys. Rev. 113, 795 (1959).
[28]K. A. Müller, in *Proceedings of the First International Conference on Paramagnetic Resonance*, Jerusalem, 1962, edited by W. Low (Academic, New York, 1963), Vol. 1, p. 17.
[29]P. S. Narayanan and K. Verdam, Z. Physik 163, 158 (1961).
[30]K. A. Müller, Th. von Waldkirch, and W. Berlinger, Solid State Commun. 9, 1097 (1971).
[31]T. C. Ensign and S. E. Stakowski, Phys. Rev. B1, 2799 (1970).
[32]A. N. Tsiken and N. A. Shtrubina, Fiz. Tverd. Tela 12, 3353 (1970) [Sov. Phys.-Solid State 12, 2723 (1971)].
[33]H. D. Megaw, Proc. Phys. Soc. (London) 58, 133 (1946).
[34]K. W. Blazey, Phys. Rev. Letters 27, 146 (1971).
[35]M. Cardona, Phys. Rev. 140, A651 (1965).
[36]S. K. Kurtz, in *Proceedings of the International Meeting on Ferroelectricity*, edited by V. Dvorak, A. Fouskova, and P. Glogar (Czechoslovakian Academy of Sciences, Prague, 1966).
[37]H. P. R. Frederikse, W. R. Hosler, and W. R. Thurber, Phys. Rev. 143, 648 (1966).
[38]O. N. Tufte and E. L. Stelzer, Phys. Rev. 141, 675 (1966).
[39]W. R. Hosler and H. P. R. Frederikse, Solid State Commun. 7, 1443 (1969).
[40]S. H. Wemple, Phys. Rev. 137, A1575 (1965).
[41]H. P. R. Frederikse and G. A. Candela, Phys. Rev. 147, 583 (1966).
[42]Z. Sroubek, Phys. Rev. B 2, 3170 (1970).
[43]H. P. R. Frederikse, W. R. Hosler, W. R. Thurber, J. Babiskin, and P. G. Siebermann, Phys. Rev. 158, 775 (1967).
[44]N. E. Phillips, B. B. Treplett, R. D. Clear, H. E. Simon, J. K. Hulm, C. K. Jones, and R. Mazelsky, in *Proceedings of the International Conference on the Science of Superconductivity*, edited by F. Chilton (North-Holland, Amsterdam, 1971).
[45]E. Ambler, J. H. Colwell, W. R. Hosler, and J. F. Schooley, Phys. Rev. 148, 280 (1966).
[46]L. S. Senhouse, G. E. Smith, and M. V. De Paolis, Phys. Rev. Letters 15, 776 (1965).
[47]W. M. Walsh, Jr., L. W. Rupp, Jr., P. S. Peercy, and L. F. Mattheiss, Bull. Am. Phys. Soc. 17, 302 (1972).
[48]K. W. Johnson and D. H. Olsen, Phys. Rev. B 3, 1244 (1970).
[49]J. C. Slater and G. F. Koster, Phys. Rev. 94, 1498 (1954).
[50]L. F. Mattheiss, Phys. Rev. B 2, 3918 (1970).
[51]J. M. Honig, J. O. Dimmock, and W. H. Kleiner, J. Chem. Phys. 50, 5232 (1968).
[52]A. Nussbaum, in *Solid State Physics*, edited by F. Seitz and D. Turnbull (Academic, New York, 1966), Vol. 18, p. 165.
[53]S. Sugano, Y. Tanabe, and H. Kamimura, *Multiplets of Transition-Metal Ions in Crystals* (Academic, New York, 1970).
[54]F. Hund, Z. Physik 94, 11 (1935). For a discussion of the method, see M. P. Tosi, in *Solid State Physics*, edited by F. Seitz and D. Turnbull (Academic, New York, 1964), Vol. 16, pp. 1–120.
[55]A. C. Switendick, Quarterly Progress Report No. 49, 1963, MIT, Cambridge, Massachusetts (unpublished).
[56]The values of $(pp\sigma)$ and $(pp\pi)$ given by Kahn and Leyendecker (Ref. 10) do not correspond to those of Switendick. This discrepancy has also been noted by Mattheiss (Ref. 8).
[57]E. A. Kraut, T. Wolfram, and W. F. Hall, Phys. Rev. B (to be published).
[58]K. A. Müller, W. Berlinger, and R. S. Rubins, Phys. Rev. 186, 361 (1969).
[59]S. Y. Tong and A. A. Maradudin, Phys. Rev. 181, 1318 (1969).
[60]T. Wolfram, Phys. Rev. Letters 29, 1383 (1972).